Implications of spatial and temporal evolutions of thermal parameters in basin modelling

L. Amir, Luis Martinez, Jean-Robert Disnar, R. Michels, J.L. Vigneresse, C. Robin, F. Guillocheau

▶ **To cite this version:**

L. Amir, Luis Martinez, Jean-Robert Disnar, R. Michels, J.L. Vigneresse, et al.. Implications of spatial and temporal evolutions of thermal parameters in basin modelling. Marine and Petroleum Geology, 2008, 25 (8), pp.759-766. 10.1016/j.marpetgeo.2008.03.006 . insu-00310852

HAL Id: insu-00310852

https://hal-insu.archives-ouvertes.fr/insu-00310852

Submitted on 11 Aug 2008

HAL is a multi-disciplinary open access archive for the deposit and dissemination of scientific research documents, whether they are published or not. The documents may come from teaching and research institutions in France or abroad, or from public or private research centers.

L'archive ouverte pluridisciplinaire **HAL**, est destinée au dépôt et à la diffusion de documents scientifiques de niveau recherche, publiés ou non, émanant des établissements d'enseignement et de recherche français ou étrangers, des laboratoires publics ou privés.

Implications of spatial and temporal evolutions of thermal parameters in basin modelling

L. Amir [a], L. Martinez[a], J.-R. Disnar[b], R. Michels[a], J.L. Vigneresse[a], C. Robin[c] and F. Guillocheau[d]

[a]UMR 7655 G2R, Henri Poincare University, Faculty of Sciences, BP 236, 54501 Vandoeuvre les Nancy, France
[b]ISTO, UMR 6113 CNRS, Orleans University, Orleans, France
[c]Laboratoire de geologie sedimentaire, Pierre et Marie Curie University, Paris VI, France
[d]UPR-4661, Rennes Geosciences, Rennes 1 University, France

Abstract

This paper presents the Paris Basin numerical modelling at a high sequential resolution scale (1–5 my). Simulations were carried out from the computation of thermal gradients and conductivities varying with the burial of genetic units. Geologic heating rates are also calculated throughout the burial of the stratigraphic sequences. Thermal energies are then deduced. The Paris Basin is well known for its hydrocarbon potential in Liassic sediments. This study is focused on an east–west cross-section through the basin. The results show spatial and temporal variations of thermal parameters from the western to the eastern part of the profile. The reactivation of Hercynian fracture systems during the Mesozoic may be responsible for the computed variations in thermal conductivities and thermal gradients. Major geodynamic events also played a role in the simulated thermal history. Variations of the thermal energy are observed and are well correlated with the burial history of the basin. We suggest linking the simulated thermal energies to the thermal cracking of the organic matter. Our results are consistent with the prediction of hydrocarbon potential in the Cretaceous period. Consequently, this approach provides new insights to improve petroleum generation modelling issues.

Keywords: Paris Basin; Organic matter; Numerical modelling; Thermal energies; Geologic heating rates

1. Introduction

During the Early Jurassic evolution phase of the Paris Basin, transgressions allowed for the deposition of open-marine clays and the development of anoxic medium conditions favourable to the preservation of organic matter (OM) and thus to the formation of hydrocarbon source rocks ([Espitalie et al., 1987], [Ziegler, 1988], [Hanzo and Espitalie, 1993] and [Disnar et al., 1996]). In the central part of the basin, the Hettangian–Sinemurian sediments are well known for their hydrocarbon potential (Espitalie et al., 1987). The Paris Basin has already been the subject of a great number of studies aiming at reconstructing its evolution and the history of hydrocarbon genesis in its oil-prone formations. As to the maturity of the organic matter, geochemical analyses indicate that in the central part of the basin, the transformation ratio reached 80% for Hettangian–Sinemurian sedimentary units, and 40% for Lower Toarcian shales (Espitalie et al., 1987). For Early Jurassic source rocks,

the major hydrocarbon expulsion phases occurred during the Late Cretaceous and the Tertiary period (Espitalie et al., 1987).

Scientists commonly use basin modelling for reconstructing thermal history and investigating hydrocarbon genesis. During the subsidence of a basin, sedimentary sequences are subjected to increasing pressure–temperature conditions. These conditions entail the rock's compaction and the simultaneous decrease in porosity and increase in thermal conductivity. Due to higher thermicity related to the burial of source rocks, thermal energy is provided to sedimentary organic matter thus generating hydrocarbons ([Tissot and Welte, 1984], [Disnar, 1986] and [Disnar, 1994]). Although most common commercially available softwares (Temispack, PetroMod, …) are powerful tools for basin modelling, we developed and used the (1D) computer program TherMO'S ([Amir, 2002] and [Amir et al., 2005]). A flow chart of the model is displayed in Fig. 1. Here, we focus on the computation of thermal parameters from burial basin simulations within a stratigraphic sequence framework.

In this paper, we present and discuss the results obtained by applying TherMO'S to 19 boreholes located in the central part of the Paris Basin and delineating an E–W cross-section (see Fig. 2) ([Amir, 2002] and [Amir et al., 2005]). The basin modelling is based on a stratigraphic sequence database built up from well logging and correlation of maximum flooding and flooding surfaces ([Robin et al., 1996] and [Robin, 1997]).

The first part of the present paper is dedicated to the methodology and the data used. The second part presents the results of the simulations. Finally, in the last section of the paper, we discuss to what extent the spatial and temporal variations of thermal parameters are related to the Paris Basin history and whether there might be implications for organic matter maturation processes.

2. Methods and data

2.1. Modelling

In this work, we used the (1D) TherMO'S software we developed to estimate the thermal parameters of the sedimentary basin at the stratigraphic scale. A detailed description of the model is published in Amir et al. (2005). The simulated burial curves are obtained from the porosity–depth empirical law as commonly used in basin modelling (Allen and Allen, 1990). Then, using calculated palaeo-porosities values, the thermal palaeo-conductivities are estimated from the geometric mean model of Vasseur et al. (1995). To reconstruct the thermal history of the basin, basal heat flux values are firstly proposed and re-adjusted throughout the thermal modelling procedure (Amir et al., 2005). For each sequence, thermal gradients and temperatures are computed from Fourier's law, using thermal palaeo-conductivities previously calculated during the burial procedure. Then, next steps of this thermal procedure are based on the Arrhenius law. In 1986, (Disnar, 1986) and (Disnar, 1994) published a model to estimate palaeo-temperatures using optimum temperatures issued from Rock-Eval pyrolysis. Here, we considered a similar modelling but we suggest deducing thermal energies according to the thermal parameters computed throughout each sequence burial simulation. Finally, the organic matter optimum thermal cracking temperatures measured in the laboratory with a Rock-Eval pyrolyzer constrain the calibration of the thermal parameters.

2.2. Data

The data we used for the Paris Basin case study involve (1) a Mesozoic stratigraphic database, (2) surface palaeo-temperatures estimated from isotopic analysis (Bowen, 1966) and (3) organic matter optimum thermal cracking temperatures issued from Rock-Eval pyrolysis (Espitalie et al., 1987).

The stratigraphic database was worked out from well-log correlations ([Robin et al., 1996] and [Robin, 1997]). Correlated for all the boreholes studied, maximum flooding surfaces (MFS) were taken as the lower limit for transgressive deposits. Similarly, the flooding surfaces (FS) were taken as the lower limit for regressive deposits. The percentage of shale recorded in the well-logs was also one of the main parameters considered for the identification of the transgressive–regressive periods. Finally, each isochron was dated with reference to Odin's (1994) dating scale. The lithologic composition for the Hettangian MFS for selected wells is shown in Fig. 3.

Organic geochemistry concepts applied to describe the sedimentary organic matter (SOM) maturation involve two main parameters, namely the optimum cracking temperature and the corresponding kinetic energy. Both these parameters are measured either from laboratory maturation experiments or by temperature-programmed Rock-Eval pyrolysis ([Espitalie et al., 1985a] and [Espitalie et al., 1985b]). In this study, we used published values for the optimum thermal cracking temperature (Espitalie et al., 1987).

3. Results

3.1. Burial history simulation

Fig. 4 shows the curves simulated for selected wells located on the cross-section. The burial sequence is marked by two main tendencies: (i) between 205 and 151.3 Ma, a fast subsidence is observed, (ii) from 151.3 Ma to 80 Ma, the burial rate slows down. Table 1 presents the burial rate spatial variation calculated for specific periods.

Distinct successively slow and fast burial phases are evidenced from the West to the East of the profile (Fig. 4). The increase of burial rate recorded within the Pliensbachian period and at the end of the Malm period looks different depending on the wells' location. Specifically, comparing the results obtained for wells A and H (Table 1), we found that the burial rate evolves differently with time and space. For example, between 202.2 and 191.9 Ma, the calculated rate is 26.6 m/My and 10.6 m/My at sites A and H, respectively.

3.2. Spatial and temporal evolutions of thermal parameters

3.2.1. Thermal conductivities

Thermal conductivities commonly increase with time during burial history (Fig. 5a). Values range from 0.8 W/m/K for Early Liassic time to 2.2 W/m/K during the Lower Cretaceous period. However, from the western to the eastern part of the profile, thermal conductivities evolve at different rates during the basin burial. The geometric mean model used to calculate thermal conductivity permits integration of mineral composition and porosity of rocks (Vasseur et al., 1995). Variations of burial entail variations in porosity. This causes lateral

conductivity changes. Hence, a spatial and temporal evolution of thermal conductivity is observed throughout the basin history.

3.2.2. Thermal gradients

The thermal gradients decrease according to the burial sequence history (Fig. 5b). However, distinct spatial and temporal evolutions are well highlighted in the western and in the eastern part of the profile. Comparing the values obtained for well A and H (Table 2), we found that the highest decrease of the thermal gradient occurred within the Liassic period, i.e. between 202.2 and 191.9 Ma. The rate of this decrease differs from well A and H. For well A, this period corresponds to one of the greatest burial rate phase (26.6 m/My) while the burial rate was only 10.6 m/My for well H. This difference results in a greater decrease of the thermal gradient for well A (24 °C/km) in comparison to well H (14.6 °C/km). From 141 to 120 Ma, we found that the decrease of the thermal gradient was very low (−0.8 °C/km for both wells) and corresponded to the finishing Malm–Lower Cretaceous period marked by the slowest burial rate estimated to 4.8 and 7.2 m/My for wells A and H, respectively. From the end of the Malm, gradient values are ranging between 30 and 50 °C/km (Fig. 5b).

3.3. Geologic heating rate and thermal energy

The modelling was carried out using the classical Arrhenius theory. The model estimates geologic heating rates, the organic matter optimum cracking temperatures, and the corresponding activation energy. The geologic heating rates are calculated from the burial rates and the thermal gradients. Thus, due to the spatial and temporal variations observed for both parameters, the geologic heating rates also display distinct lateral and vertical evolution (Fig. 6). The data shown in Table 3 indicate the influence of geologic heating rate variations on the energies estimated for wells A and H. Throughout the burial history, we found distinct geologic heating rates ranging between 0.03 °C/My and 10.9 °C/My. The results also indicate that increasing the heating rate also decreases the energy, and the conversely is also true.

Distinct evolutions are observed between wells A and H. Furthermore, we notice that variations of the heating rates occur within very short time intervals (Table 3). For example, between 187.5 and 187.2 Ma (time interval: 0.3 my), an increase of the heating rates is estimated at 5.7 °C/My resulting in a decrease by 1.3 kcal/mol for the energy. Between 160.9 and 159.4 Ma, an increase of 6 °C/My for the geologic heating rates is immediately followed by a decrease of the same amount for well A. For well H, the same evolution is observed although the amount of increase is weaker (3 °C/My). For both cases, this causes a variation of the energy by 1–2 kcal/mol. The most important variation occurs during the Malm. At 151.3 Ma, we found the heating rates increase by 10.9 °C/My and 5 °C/My, for wells A and H respectively. Consequently, the energy decreases by 2 kcal/mol for both wells. Finally, from the Lower Cretaceous, the energies are estimated between 46 and 49 kcal/mol. The corresponding geologic heating rates all range below 2 °C/My.

4. Discussion

Basin analysis typically considers constant or linear thermal gradients. In this work, the computation of the thermal gradients takes into account the spatial and temporal variations of thermal conductivities. This approach permits the estimation of thermal energies from the spatial and temporal variations of the geologic heating rates.

Previously published data largely agree with the results obtained. Considering all the Liassic horizons penetrated by well A, the mean thermal gradient we computed also matches with previous studies dealing with the present day thermal regime of the Paris Basin (50–70 °C/km) ([Amir et al., 2005] and [Gaulier and Burrus, 1994]).

Variations in burial rates and effects on the simulated thermal parameters can be explained from published geodynamic investigations on the Paris Basin. In 1980, Megnien suggested the occurrence of syn-sedimentary faulting and more generally reactivation of Hercynian structures during the Pliensbachian stage. Later, Ziegler (2005) underlined the occurrence of repeated Mesozoic reactivation of fracture systems transecting the Paris Basin. He also emphasised the control of subsidence by geodynamic processes from the Permian to Early Cretaceous times. Finally, he suggested the occurrence of a Stephanian–Permian tectono-magmatic event followed by thermal subsidence. This could explain the high thermal gradient values we estimated in our modelling for the Liassic period. Episodes of thermal anomalies during the basin evolution were also suggested in other studies based on clay minerals experiments ([Spötl et al., 1996] and [Liewig et al., 1987]).

The major contribution of this work deals with the modelling of spatial and temporal variations of thermal energies according to the basin history. The great issue concerns the possible influence on chemical reactions and organic matter thermal cracking in particular. During its thermal degradation, the organic matter evolves depending on distinct molecular hydrocarbon classes basically depending on its composition. Consequently, the question of frequency factor choice in the Arrhenius law is complex. To reproduce the formation of each component type issued from the thermal cracking of the sedimentary organic matter, scientists use distinct frequency factors ([Ungerer et al., 1988], [Behar et al., 1988] and [Behar et al., 1992]; Burnham and Sweeney, 1989; [Burnham and Braun, 1990], [Vandenbroucke et al., 1999] and [Al Darouich, 2005]). Here, we use a constant frequency factor for the whole study and focus on the temporal variation for the thermal energy distribution. The results obtained show that thermal energies values computed for the end of the Malm–lower Cretaceous interval are consistent with kinetic models favourable for hydrocarbon genesis. Moreover, according to Espitalie et al. (1987), hydrocarbon production began in the Cretaceous period.

5. Conclusion

Understanding the temporal and spatial variations of thermal parameters in basin modelling has implications for petroleum issues. Experimental and fundamental research show that thermal cracking of the organic matter depends on the heating rate. Thermal parameters recorded within sedimentary deposits constrain organic and mineral reactions occurring during the formation and evolution of a basin. The key objective of this work was to seek how far spatial and temporal variations of thermal conductivity and thermal gradient affect the kinetic transformation of the sedimentary organic matter. This approach permits the calculation of thermal energies that can be linked to occurrence of chemical reactions in case they correspond to activation energies. The comparison between the thermal energy values provided by burial history and tectonics, and activation energies measured in laboratory experiments, might help to better assess and constrain kinetic distribution models. In this work, the variations of the thermal parameters directly relate to syn-sedimentary tectonics and geodynamic processes. Kinetic computational modelling could be considerably improved. Finally, kinetic energy models computed according to basin history might also help to estimate the timing of organic–inorganic interactions within a stratigraphic sequence framework.

Acknowledgments

We greatly acknowledge Sophie Violette and the French PNRH-99 program for their support of this work. The first author also thanks Ziegler P.A., Isabel Suarez-Ruiz Isabel, D.G. Roberts and an anonymous reviewer for their comments that led to the improvement of the present article.

References

Al Darouich, 2005 Al Darouich, T., 2005. Stabilité thermique de la fraction aromatique de l'huile brute Safaniya (Moyen Orient):étude expérimentale, schéma cinétique par classes moléculaires et implications géochimiques, PhD thesis, Paris 6 University, France, p. 225.

Allen and Allen, 1990 P.A Allen and J.R. Allen, Basin Analysis: Principles and Applications, Blackwell Scientific Publications Cambridge (1990) 451 pp..

Amir, 2002 Amir, L., 2002. Modélisation thermique appliquée aux basins sédimentaires et utilisant la géochimie organique: Conception du logiciel «TherMO'S» pour la reconstitution de l'histoire thermique du Bassin Parisien à l'échelle séquentielle, PhD thesis, Henri Poincaré University, Nancy, France, 161 pp.

Amir et al., 2005 L. Amir, L. Martinez, J.-R. Disnar, J.-L. Vigneresse, R. Michels, F. Guillocheau and C. Robin, Effect of the thermal gradient variation through geological time on basin modeling; a case study: the Paris basin, *Tectonophysics* **400** (2005), pp. 227–240.

Behar et al., 1988 Behar, F., Ungerer, P., Audibert, A., Villalba, M., 1988. Experimental study and kinetic modelling of crude oil pyrolysis in relation to thermal recovery processes. In: 4th International Conference on Heavy Crude Oil and Tar Sands, Edmond, Canada, pp. 747–759.

Behar et al., 1992 F. Behar, S. Kressman, J.L. Rudkiewicz and M. Vandenbroucke, Experimental simulation in a confined system and kinetic modelling of kerogens and oil cracking, *Organic Geochemistry* **19** (1992), pp. 173–189.

Bowen, 1966 R. Bowen, Paleotemperature analysis, *Methods in Geochemistry and Geophysics* **vol. 2**, Elsevier, Amsterdam (1966) 139 pp..

Burnham and Braun, 1990 A.K. Burnham and R.L. Braun, Development of a detailed model of petroleum formation, destruction and expulsion from lacustrine and marine source rocks, *Organic Geochemistry* **16** (1990), pp. 27–39.

A.K. Burnham and J.J. Sweeney, A chemical kinetic model of vitrinite reflectance maturation, *Geochimica et Cosmochimica Acta* **53** (1989), pp. 2649–2657.

Disnar, 1986 J.R. Disnar, Détermination de paléo températures maximales d'enfouissement de sédiments charbonneux à partir de données de pyrolyse, *Comptes Rendus de l'Académie des Sciences, Paris. Série 2. Sciences de la Terre et des Planètes* **303** (8) (1986), pp. 691–696.

Disnar, 1994 J.R. Disnar, Determination of maximum paleotemperatures of burial (MPTB) of sedimentary rocks from pyrolysis data on the associated organic matter: basic principles and practical application, *Chemical Geology* **118** (1994), pp.

Disnar et al., 1996 J.-R. Disnar, P. Le Strat, G. Farjanel and A. Fikri, Organic matter sedimentation in the northeast of the Paris Basin: consequences on the deposition of the lower Toarcian Black Shales, *Chemical Geology* **131** (1996), pp. 15–35.

Espitalie et al., 1985a J. Espitalie, G. Deroo and F. Marquis, La pyrolyse Rock-Eval et ses applications, *Revue de l'Institut Français du Pétrole* **40** (1985), pp. 563–579.

Espitalie et al., 1985b Espitalie, J., Deroo, G., Marquis, F., 1985b. Rock Eval pyrolysis and its application. 27299, Projet B41 79008, IFP Géologie et Géochimie.

Espitalie et al., 1987 J. Espitalie, F. Marquis, L. Sage and I. Barsony, Géochimie organique du bassin de Paris, *Revue de l'Institut Français du Pétrole* **42** (3) (1987), pp. 271–302.

Gaulier and Burrus, 1994 J.M. Gaulier and J. Burrus, Modeling present and past thermal regimes in the Paris Basin: petroleum implications. In: A. Mascle, Editor, *Hydrocarbon and Petroleum Geology of France*, Springer-Verlag, Berlin (1994), pp. 61–73.

Hanzo and Espitalie, 1993 M. Hanzo and J. Espitalie, Relation entre matière organique et sédimentation dans le Lias de Lorraine (France), *Comptes Rendus de l'Académie des Sciences, Paris* **316** (1993), pp. 945–950.

Liewig et al., 1987 N. Liewig, J.R. Mossman and N. Clauer, Datation isotopique K-Ar d'argiles diagenetiques de reservoirs greseux: mise en evidence d'anomalies thermiques du Lias inferieur en Europe nord-occidentale, *Comptes Rendus de l'Académie des Sciences, Paris. Serie 2, Sciences de la Terre et des Planètes* **304** (13) (1987), pp. 707–709.

Megnien, 1980 C. Megnien, Tectogénèse du Bassin de Paris: Etapes de l'évolution du Bassin, *Bulletin de la Société Géologique de France* **XXII** (4) (1980), pp. 669–680.

Odin, 1994 G.S. Odin, Geological time scale, *Comptes Rendus de l'Académie des Sciences de Paris* **318** (1994), pp. 59–71.

Robin et al., 1996 C. Robin, F. Guillocheau and J.-M. Gaulier, Mesure des signaux eustatiques et tectoniques au sein de l'enregistrement d'un bassin intracratonique. Application au Lias du Bassin de Paris, *Comptes Rendus de l'Académie des Sciences de Paris, IIa* **322** (1996), pp. 1079–1086.

Robin, 1997 Robin, C., 1997. Mesure stratigraphique de la déformation: Application à l'évolution Jurassique du bassin de Paris. Doctorat Thesis, Rennes 1, Rennes, 293 pp.

Spötl et al., 1996 C. Spötl, R.H. Worden and F. Walgenwitz, Clay mineralogy as records of temperature conditions and duration of thermal anomalies in the Paris Basin, France: discussion, *Clay Minerals* **31** (1996), pp. 203–208.

Tissot and Welte, 1984 B.P. Tissot and D.H. Welte, Petroleum Formation and Occurrence, Springer-Verlag, Berlin (1984).
Ungerer et al., 1988 P. Ungerer, F. Behar, M. Villalba and O.R. Heum, Kinetic modeling of oil cracking, *Organic Geochemistry* **13** (1988), pp. 857–868.

Vandenbroucke et al., 1999 M. Vandenbroucke, F. Behar and J.L. Rudkiewicz, Kinetic modeling of petroleum formation and cracking: implication from the high pressure/high temperature Elgin Field (UK, North Sea), *Organic Geochemistry* **30** (1999), pp. 1105–1125.

Vasseur et al., 1995 G. Vasseur, F. Brigaud and L. Demongodin, Thermal conductivity estimation in sedimentary basins, *Tectonophysics* **244** (1995), pp. 167–174.

Ziegler, 1988 P.A. Ziegler, Evolution of the Arctic–North Atlantic and the Western Tethys, *American Association of Petroleum Geologists, Memoirs* **43** (1988), p. 198.

Ziegler, 2005 P.A. Ziegler, Permian to recent evolution, *Europe/Permian to Recent Evolution*, Elsevier (2005), pp. 102–125.

Figures and Tables

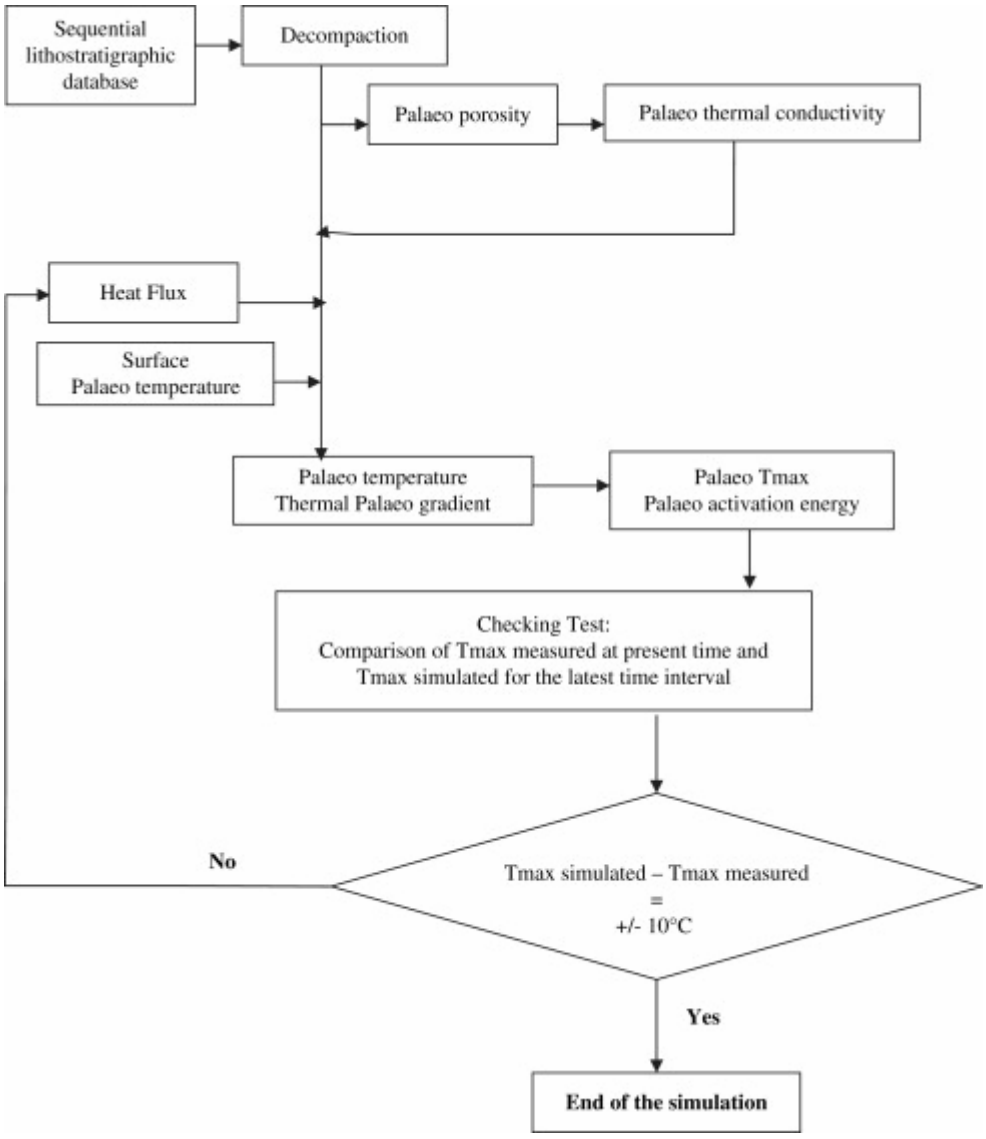

Fig. 1. Flow chart of the TherMO'S computer program. T_{max} corresponds to the optimum thermal cracking temperature of the organic matter.

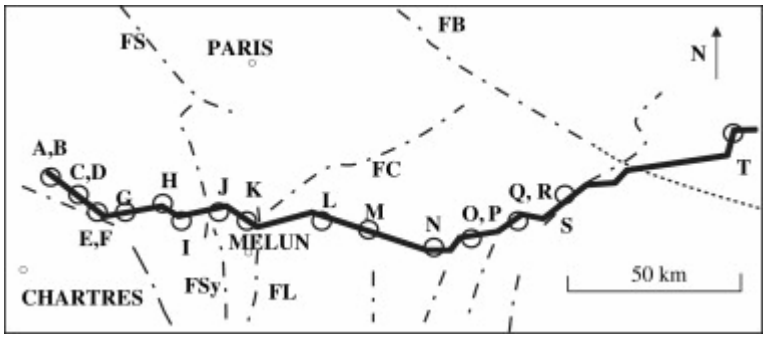

Fig. 2. Boreholes location on the E–W studied cross-section. Faults are represented by bold dashed lines (FS: Seine Fault; FSy: Sennely Fault; FL: Loire Faut; FC: Chaunoy Fault; FB: Bray Fault; FStMBos: St Martin de Bossenay Fault).

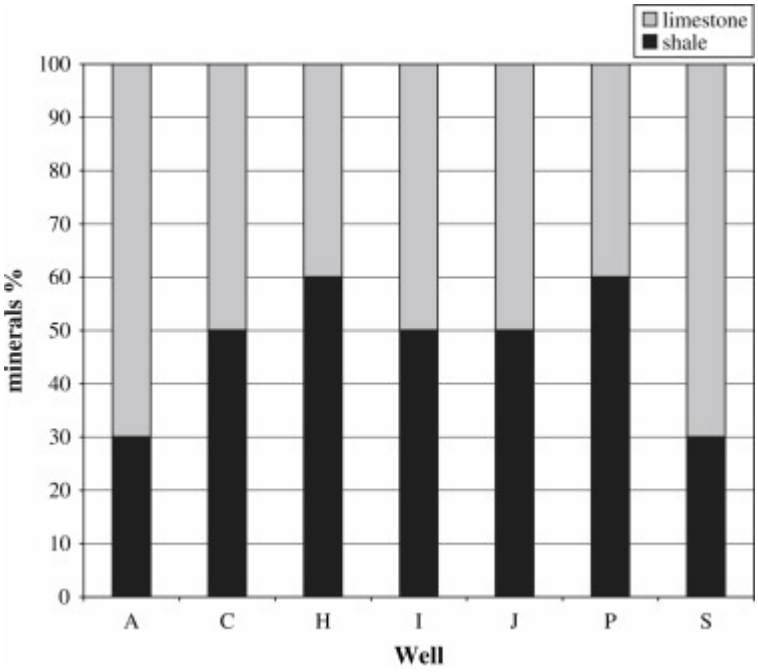

Fig. 3. Lithologic composition for the H1 isochron representing the lower limit of the mid-transgressive Hettangian sequence. The histogram shows the percentage of shale and limestone recorded for selected boreholes located within the E–W transect.

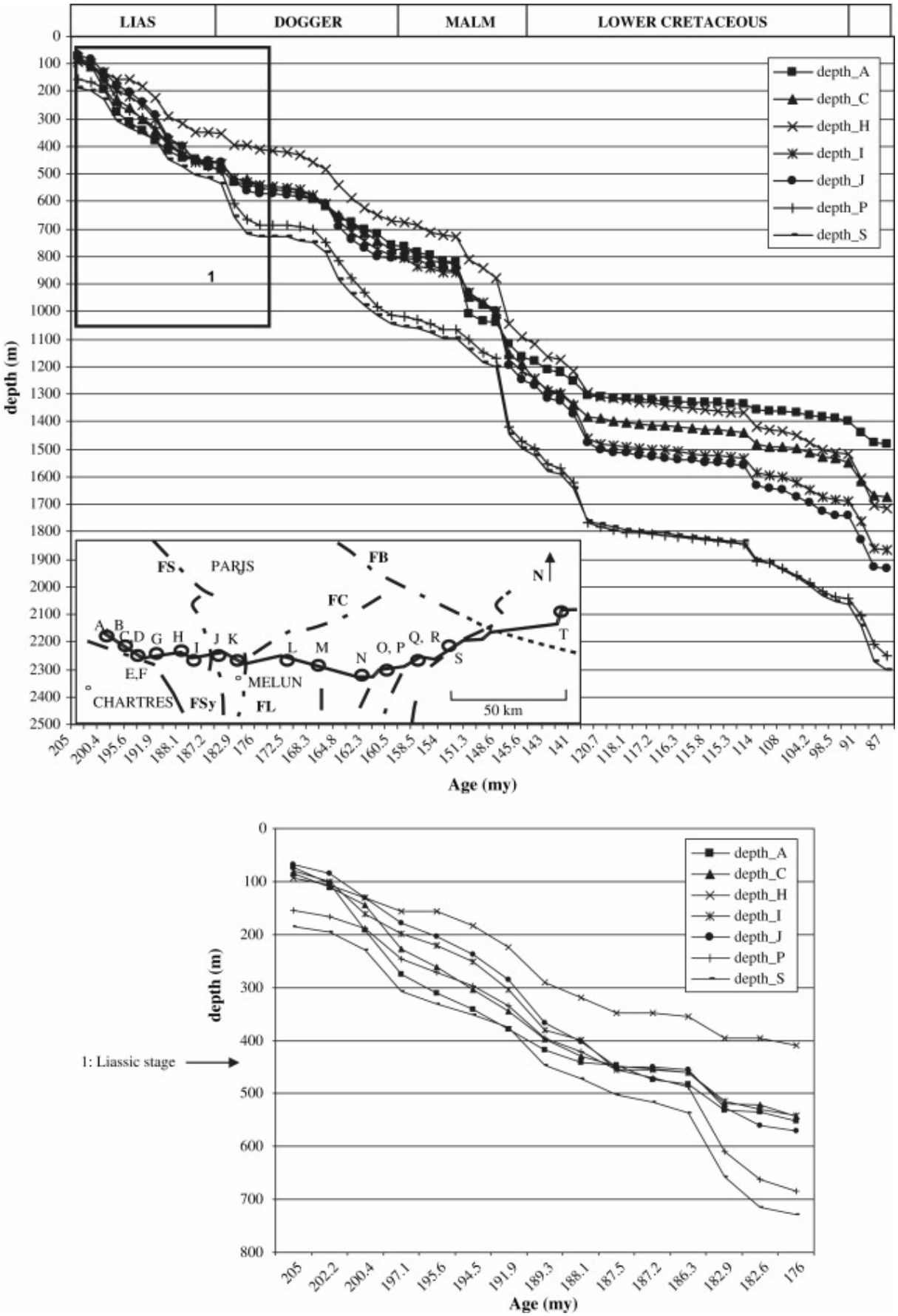

Fig. 4. Simulation of the burial history for the mid-transgressive Hettangian deposits for selected wells along the E–W profile.

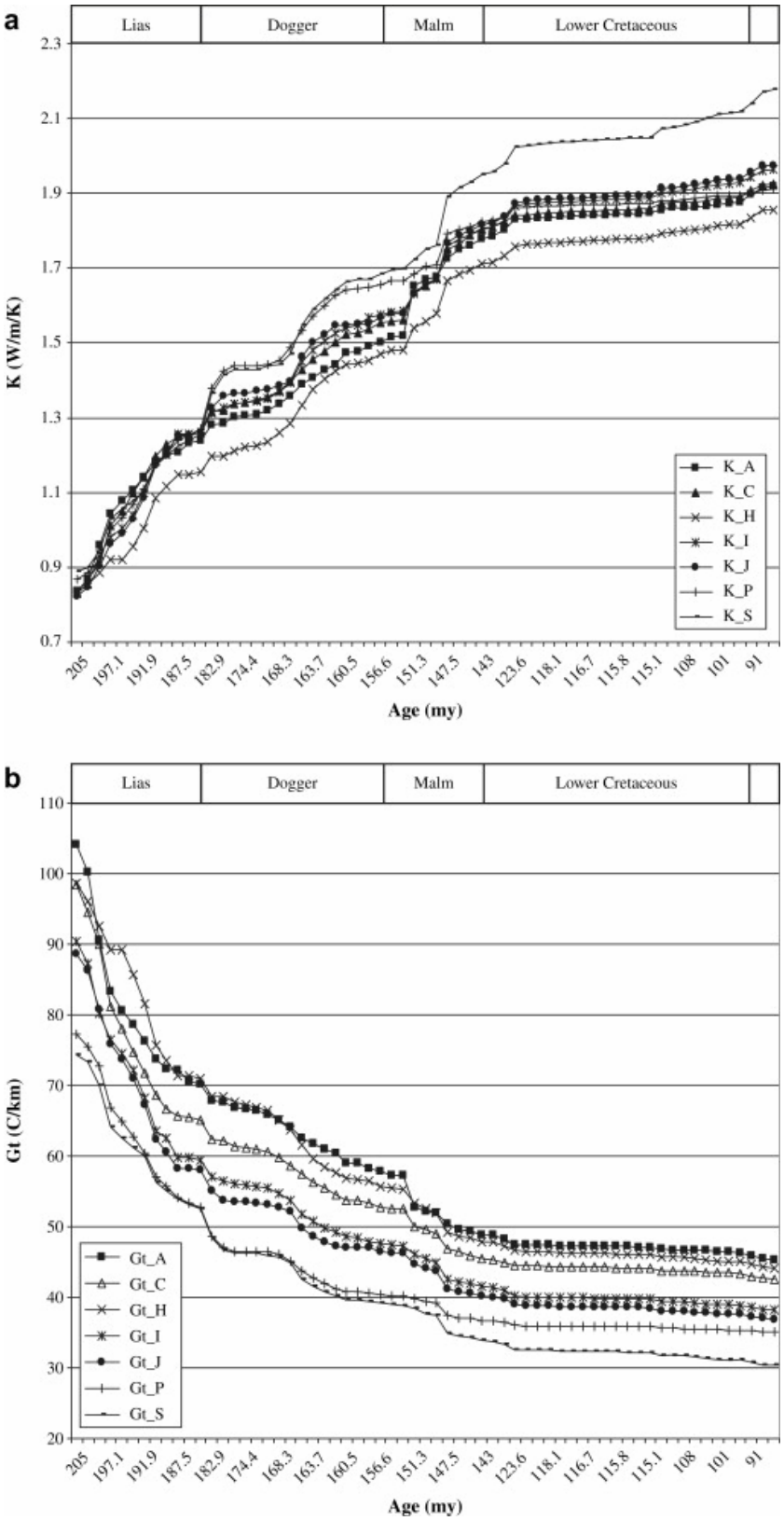

Fig. 5. (a) Simulation of the thermal conductivities evolution throughout the burial history of the mid-transgressive Hettangian deposits for selected wells along the profile; (b) simulation of the thermal gradients evolution throughout the burial history of the mid-transgressive Hettangian deposits for selected wells along the profile.

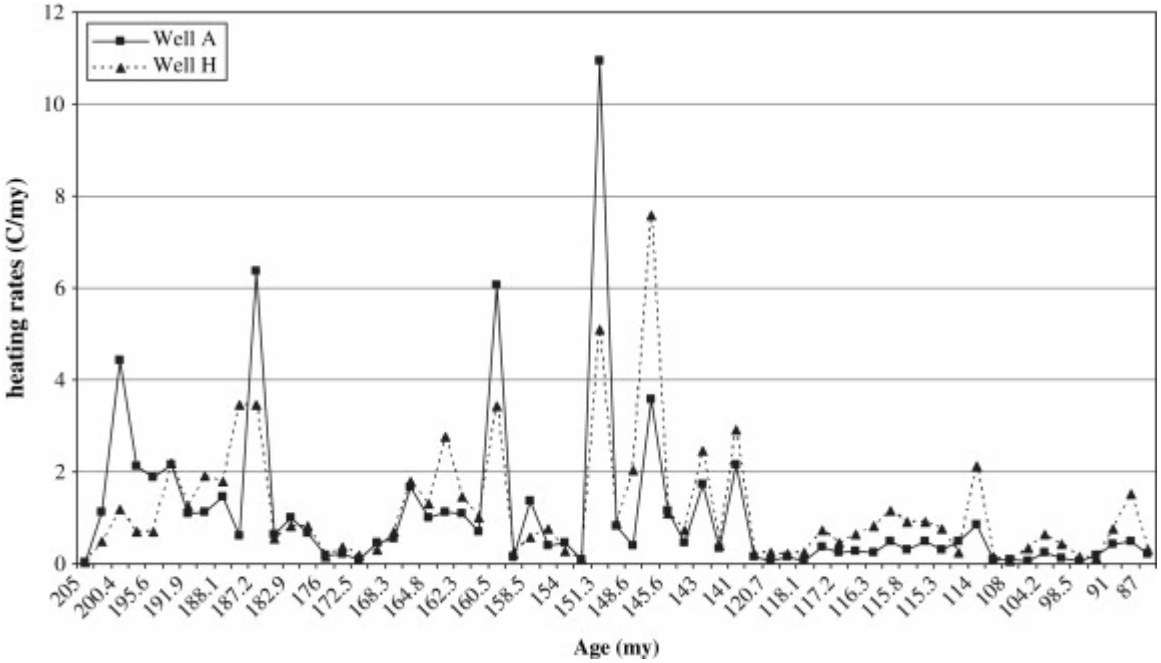

Fig. 6. Geologic heating rates computed with TherMO'S for wells A and H.

Table 1. : Variation of the burial rate along the profile

Period (my)	**Time interval (my)**	**Results: burial rate (m/my)**						
		Well A	**Well C**	**Well H**	**Well I**	**Well J**	**Well P**	**Well S**
202.2–191.9	10.3	26.6	22.7	10.6	19.7	19.5	16.3	17.6
188.1–176	12.1	9.1	9.3	21.2	11.7	13.9	21.7	21.2
176–168.3	7.7	5.2	4.8	6.2	4.8	3.1	2.1	2.5
168.3–160.5	7.8	21.5	24.7	27.6	28.1	26.9	40.0	38.3
160.5–151.3	9.2	26.8	18.7	15.3	14.7	13.8	9.6	9.8
151.3–143	8.3	24.7	41.1	42.0	43.1	46.5	54.8	53.1
141–120.7	20.3	4.8	5.1	7.2	9.3	9.1	11.3	9.6
120.7–104.2	16.5	4.0	7.4	10.1	10.2	11.7	12.1	13.5
104.2–87	17.2	6.1	9.5	14.0	12.8	14.1	15.5	18.0

Rates of burial are expressed in m/my.

Table 2. : Effects of the burial rate variations on thermal parameters computed with TherMO'S

Time interval (my)	**Burial rate (m/my)**		**Δ*K* (W/m/K)**		**ΔGt (°C/km)**	
	Well A	**Well H**	**Well A**	**Well H**	**Well A**	**Well H**
202.2–191.9	26.6	10.6	(+) 0.27	(+) 0.15	(−) 24	(−) 14.6
188.1–176	9.1	21.2	(+) 0.1	(+) 0.08	(−) 5.5	(−) 5.7
176–168.3	5.2	6.2	(+) 0.03	(+) 0.06	(−) 1.8	(−) 2.6
168.3–160.5	21.5	27.5	(+) 0.14	(+) 0.18	(−) 6	(−) 8.2
160.5–151.3	26.8	15.3	(+) 0.18	(+) 0.1	(−) 6.4	(−) 3.6
151.3–143	24.7	42	(+) 0.13	(+) 0.17	(−) 3.7	(−) 5.4
141–120.7	4.8	7.2	(+) 0.03	(+) 0.03	(−) 0.8	(−) 0.8
120.7–104.2	4	10.1	(+) 0.04	(+) 0.04	(−) 0.9	(−) 1.1
104.2–87	6.1	14	(+) 0.03	(+) 0.05	(−) 1.2	(−) 1.2

Table 3. : Effects of the geologic heating rate variations on the thermal energies estimations

Age (my)	**Geologic heating rates (°C/my)**		**Thermal energy (kcal/mol)**	
	Well A	**Well H**	**Well A**	**Well H**
205	0.037	0.045	40.269	40.339
202.2	1.109	0.481	38.664	39.082
200.4	4.427	1.183	38.873	38.803
197.1	2.121	0.702	40.199	39.431
195.6	1.883	0.702	40.548	39.431
194.5	2.143	2.180	40.758	39.013
191.9	1.084	1.254	41.596	39.78
189.3	1.134	1.921	41.945	40.129
188.1	1.447	1.775	42.015	40.478
187.5	0.601	3.454	42.644	40.339
187.2	6.359	3.454	41.316	40.339
186.3	0.625	0.552	42.994	41.666
182.9	0.997	0.806	43.134	41.806

Age (my)	Geologic heating rates (°C/my)		Thermal energy (kcal/mol)	
	Well A	Well H	Well A	Well H
182.6	0.677	0.806	43.414	41.806
176	0.172	0.144	43.974	42.505
174.4	0.208	0.378	43.834	41.945
172.5	0.105	0.176	44.324	42.435
170.6	0.451	0.315	42.994	41.666
168.3	0.538	0.708	42.994	41.316
167.3	1.666	1.787	42.505	40.967
164.8	1.001	1.305	42.505	40.967
163.7	1.124	2.761	42.575	40.827
162.3	1.088	1.459	42.784	41.596
160.9	0.690	0.987	43.204	42.015
160.5	6.051	3.412	42.015	41.386
159.4	0.161	0.206	44.534	43.274
158.5	1.360	0.565	43.274	42.644
156.6	0.396	0.763	44.184	42.644
154	0.441	0.277	44.254	43.414
152.2	0.095	0.092	45.304	44.184
151.3	10.940	5.090	43.414	42.085
149.5	0.810	0.877	45.444	43.414
148.6	0.404	2.021	46.004	43.204
147.5	3.577	7.567	44.954	43.344
145.6	1.150	1.102	46.074	44.954
143.9	0.465	0.740	46.845	45.444
143	1.738	2.447	46.145	44.884
141.7	0.338	0.404	47.406	46.285
141	2.138	2.907	46.215	45.094
123.6	0.147	0.206	47.617	46.425

Age (my)	Geologic heating rates (°C/my)		Thermal energy (kcal/mol)	
	Well A	**Well H**	**Well A**	**Well H**
120.7	0.049	0.241	48.459	46.215
119.1	0.148	0.203	47.617	46.355
118.1	0.047	0.232	48.459	46.215
117.6	0.379	0.742	46.916	45.374
117.2	0.237	0.463	47.266	45.724
116.7	0.284	0.648	47.126	45.584
116.3	0.236	0.809	47.266	45.514
116.1	0.472	1.154	46.775	45.304
115.8	0.315	0.923	47.126	45.514
115.6	0.472	0.922	46.845	45.584
115.3	0.314	0.768	47.196	45.724
115.1	0.471	0.230	46.916	46.635
114	0.852	2.119	46.565	45.094
110.7	0.099	0.166	48.178	46.986
108	0.099	0.068	48.178	47.617
106	0.070	0.341	48.388	46.495
104.2	0.233	0.630	47.547	46.145
101	0.116	0.424	48.038	46.495
98.5	0.074	0.144	48.388	47.336
96	0.185	0.126	47.757	47.476
91	0.412	0.768	47.617	47.126
88	0.500	1.504	47.827	47.547
87	0.227	0.309	48.459	48.739

The pre-exponential coefficient is $A0 = 1.6 \times 10^{14}$ (type II – organic matter, marine origin).